Electronic Supplementary Information (ESI)

Hexaazatrinaphthylene Based Near-infrared Photothermal Organic-Small-Molecule for Efficient Photo-Thermo-Electric Conversion

Ning-Ning Zhang,[a,b] Wei-Li Zheng,[a] Lin-Xu Liu,[a] Rong Ma,[a] Zhenyu Li,[c,d] Yongfang Han,[a] Wen-Wen Zi,[a] and Yong Yan*[a,d]*

[a]School of Chemistry and Chemical Engineering, Liaocheng University, Liaocheng, Shandong 252000, P. R. China.

[b]Fujian Key Laboratory of Advanced Inorganic Oxygenated Materials, Fuzhou University, Fuzhou, Fujian 350108, P. R. China.

[c]School of Environmental and Materials Engineering, Yantai University, Yantai, 264005, P. R. China.

[d]State Key Laboratory of Structural Chemistry, Fujian Institute of Research on the Structure of Matter, Chinese Academy of Sciences, Fuzhou, Fujian 350108, P. R. China.

**Email: zhangningning@lcu.edu.cn (N. N. Zhang); yanyong@lcu.edu.cn (Y. Yan)*

1. Experimental section

Materials. All reagents were obtained from commercial sources and used without further purification. **HTA** was synthesized following a previously reported procedure.[1] The phase purity of **HTA** was confirmed by infrared (IR) spectrum (Fig. S1).

Measurements. Diffuse reflectance spectrum was measured at room temperature over the 250–1500 nm range using a Shimadzu UV-3600i Plus spectrophotometer equipped with an integrating sphere. A $BaSO_4$ plate was employed as the reference (100% reflectance), and finely ground sample powders were coated directly onto the reference plate. Electron paramagnetic resonance (EPR) spectra were recorded on a CIQTEK EPR-200Plus spectrometer operating in the X-band with a 100 kHz magnetic field modulation. Fourier-transform infrared (IR) spectra were collected in the range of 4000 to 400 cm^{-1} on a Nicolet iS50 spectrometer.

The NIR photothermal conversion measurement. NIR-I/II photothermal conversion measurements were conducted by pressed pellets of **HTA** with lasers of 808 nm and 1064 nm produced by Changchun New Industries Optoelectronics Tech. Co., Ltd, respectively. The temperature of samples was recorded by a HIKMICRO K20 infrared camera. The temperature detecting range of the infrared camera was set as auto. The sample pellet with a diameter of 5 mm and a weight of 15.9 mg was prepared using a tablet press.

The photo-thermo-electric conversion measurement. The photo-thermo-electric conversion of **HTA** was investigated by integrating its sample powder with a commercial thermoelectric generator. Approximately 50 mg of **HTA** powder was uniformly coated onto the surface of the thermoelectric chip using a thin layer of thermally conductive adhesive. Simulated solar irradiation at intensities of 1 Sun (1000 W/m^2), 2 Suns (2000 W/m^2) and 4 Suns (4000 W/m^2)

were provided by a xenon lamp (CEL-PF300-T9, CEAULIGHT) equipped with an attenuator, and the light intensity was measured using a TES1333 solar power meter. Three thermoelectric devices—TEC1-12701 (40 × 40 × 5.2 mm^3), TEC1-12703 (40 × 40 × 4.4 mm^3), and TEC1-12706 (40 × 40 × 3.8 mm^3)—served as thermoelectric generators. The open-circuit voltage and current were measured with a Keithley 2450 source meter. Surface temperature variations during illumination were monitored using a HIKMICRO K20 infrared thermal camera.

Calculation of optical absorption lines and spin density. The structural models of g-**HTA,** s-[**HTA**]$^{\bullet\bullet}$ and t-[**HTA**]$^{\bullet\bullet}$ were constructed in GaussView 5.0 and optimized using the B3LYP[2] function with the 6-311G(d,p) basis set in Gaussian 16,[3] followed by time-dependent density functional theory (TD-DFT) calculations. The resulting wavefunction data were all analyzed using the Multiwfn program.[4]

2. Additional tables and graphics

Table S1. Reported photothermal materials and their performance in photo-thermo-electric conversion when integrating with thermoelectric generators under the irradiation of 1 Sun.

Items	Photo-thermo-electric conversion (under 1 Sun)		Reference
	Open circuit voltage (mV)	Maximum output power density (W/m^2)	
Organic-small-molecule photothermal materials			
HTA	211	0.69	**This work**
DDPA-PDN	83	/	*Adv. Funct. Mater.* **2021**, 2106247
GDPA-QCN	58	/	*Angew. Chem. Int. Ed.* **2022**, e202117087
Organic cocrystal photothermal materials			
TQC	427	1.31	*ACS Energy Lett.* **2023**, 8, 4179−4185.
Organic-inorganic hybrid photothermal materials			
$\{[BaMn(ONDI)_2(H_2O)_3]\cdot H_2O\}_n$	313	0.873	*Chem. Eng. J.* **2024**, 491, 152054.
$\{[Ni_4Cl_2(ONDI)_2(bpy)_4]\cdot 2Cl\cdot 2H_2O\cdot xDMF\cdot y H_2O\}_n$	250	0.53	*Chem. Eng. J.* **2024**, 499, 156059.
Inorganic photothermal materials			
NF@RGO-CNT	58-59	0.251	*Ind. Eng. Chem. Res.* **2022**, 61, 16565−16576.
Ni_3S_2/NF	59	0.175	*ACS Sustain. Chem. Eng.* **2020**, 8, 10833−10841.
CNT foam/PVA	96.35	0.4	*ACS Appl. Nano Mater.* **2021**, 4, 8906−8912.
PNPG/MoS_2	110	0.23	*ACS Appl. Mater. Interfaces.*

			2022, 14, 1034−1044.
3D porous CPP	19.76	0.5	*ACS Sustain. Chem. Eng.* **2021**, *9*, 4571–4582.
PCC sponge	60	0.4	*Adv. Energy Mater.* **2019**, 1900250
CNTP	100	0.24	*Energy Convers. Manag.* **2021**, 241, 114306.
MnO/C-600	177	0.77	*Chem. Eng. J.* **2023**, 451, 138534.
MC10	168.3	0.6	*Energy Environ. Mater.* **2022**, 0, 1–9.
PC-x hydrogels	165.8	0.65	*Chem. Eng. J.* **2023**, 458, 141511.
PCC-800	201	0.8	*ACS Sustain. Chem. Eng.* **2022**, 10, 16427−16439.
MoS_2-x NSAs	98.2	0.749	*Energy Convers. Manag.* **2022**, 252, 115070.
MSx-CPC	110	1.087	*Small* **2022**, 18, 2201949.
T-MSMD	89	0.721	*ACS Appl. Mater. Interfaces* **2021**, 13, 4305−4315.
Polymer photothermal materials			
CP@PVA	112.9	1.04	*Sci. China Mater.* **2022**, 65, 2491–2501.

Table S2. Reported NIR-II photothermal materials and their photothermal conversion efficiency (PCE, η) under the irradiation of a 1064 nm laser.

Items	η_{1064}	**Reference**
Organic-small-molecules		
BAF4	80 %	*Angew. Chem. Int. Ed.*, **2021**, 60, 22376–22384
CY-1234	76.01 %	*Small*, **2023**, 2307829
2	62.26 %	*Angew. Chem. Int. Ed.*, **2024**, e202400913
HTA	**61.68 %**	**This work**
Zn_4-H_2Pc/DP	58.3 %	*Chem. Sci.*, **2019**, 10, 8246–8252
DAF-OH_2⊂GBox-4^{4+}	47.4 %	*Angew. Chem. Int. Ed.*, **2023**, 135, e202301267
DAF_2⊂GBox-4^{4+}	37.6%	
TTF_2⊂GBox-4^{4+}	39.9%	
CSM_2	31.6 %	*Mater. Horiz.*, **2020**, 7, 1379–1386
COFs		
CNPs	50.6 %	*Chem. Commun.*, **2020**, 56, 7793−7796
Py-BPy-COF NPs	55.2 %	*J. Am. Chem. Soc.*, **2019**, 141, 14433–14442
HOFs		
TQC@PFC-1	32 %	*J. Mater. Chem. B*, **2023**, 11, 8649−8656
Complexes		
$[Sr(BCA)_2(H_2O)_2]_n$	84.5 %	*Inorg. Chem. Front.*, **2024**, 11, 4867–4875
Cu-THQNPs	51.34%	*ACS Appl. Mater. Interfaces*, **2018**, 10, 25203–25212
Au@MOF	48.5%	*Nano Lett.*, **2019**, 19, 6772–6780
rPMo·cTMB	48.4 %	*Adv. Healthcare Mater.*, **2022**, 11, 2102352
pMOF-a	32.2 %	*Chem. Commun.*, **2022**, 58, 11095–11098
THPTS-Pb	15.2 %	*Inorg. Chem.*, **2024**, 63, 3327–3334
Polymers		

Y1	67.9 %	*Chem. Sci.,* **2021**, 12, 5177–5184
Y2	69.5 %	
Y3	76.5%	
PBBTDTS	65.0 %	*Chem. Commun.*, **2020**, 56, 1093–1096
SPNs3	60.0 %	*Chem. Commun.*, **2019**, 55, 9487–9490
HPW@PANI	57.76 %	*Int. J. Nanomed.*, **2022**, 17, 5565–5579
$2MPT^{2+\bullet}CB$	54.6 %	*Angew. Chem., Int. Ed.*, **2019**, 58, 15526–15531
N1@2P	53.8 %	*Small,* **2023**, 19, 2300203
P_3	46.0 %	*ACS Nano*, **2019**, 13, 7345–7354
$NP^{PSP\text{-}P}t$	43.2 %	*Adv. Mater.,* **2023**, 35, 2300048
2NDTA	35 %	*Adv. Funct. Mater.,* **2024**, 2401627
SPNs	21.2 %	*ACS Appl. Mater. Interfaces,* **2020**, 12, 33492–33499.
SP1	2.3 %	*Angew. Chem.Int. Ed.,* **2023**, 62, e202301617
SP2	46.4 %	
SP3	44.9 %	
SP4	46.5 %	
SP5	42.4 %	
Inorganic materials		
N-Doping CDs	81.3 %	*Carbon*, **2020**, 162, 220–233
AuPBs	80.8 %	*ACS Nano*, **2018**, 12, 2643–2651
Au_3Cu nanocrystals	75.2 %	*Nanoscale Horiz.*, **2018**, 3, 624–631
MoO_2 NPs	55.6 %	*Sci. China Mater.*, **2020**, 63, 1085–1098
CS–RuO_2 NPs	52.5 %	*Chem. Commun.*, **2020**, 56, 3019–3022
Pd Ncap	49.2 %	*ACS Appl. Mater. Interfaces*, **2023**, 15, 39081–39098
Sb-Doped SnO_2	48.3 %	*Nanoscale*, **2018**, 10, 2542–2554
Ni_9S_8	46.0 %	*Nanoscale*, **2019**, 11, 20161–20170
Nb_2C (MXene)	45.6 %	*J. Am. Chem. Soc.*, **2017**, 139, 16235–16247

V_2C	45.0 %	*ACS Nano*, **2019**, 13, 1499–1510
$TeO_2/(NH_4)_xWO_3$ nanoribbons	43.6 %	*Nano Lett.*, **2019**, 19, 1179–1189
NIR-II-CD/BP hybrids	28.4 %	*ACS Appl. Mater. Interfaces*, **2019**, 11, 44949–44960
Si–Au	24.1 %	*J. Mater. Chem. B*, **2019**, 7, 4393–4401
EGaIn @SiO_2-RGD	22.43 %	*Nano Lett.*, **2019**, 19, 2128–2137
SnSe–PVP nanorods	20.3 %	*Mater. Horiz.*, **2018**, 5, 946–952
Au NSs	13.0 %	*J. Mater. Chem. B*, **2019**, 7, 2001–2008

Table S3 List of the triplet diradical states for t-**[HTA]$^{\bullet\bullet}$** (the lowest singly unoccupied molecular orbital (SUMO) and the singly occupied molecular orbital (SOMO))

Excited State	**Wavelength (nm)**	**Oscillator strength**	**Electronic transition (%)**
4	**1186.14 nm**	0.0056	β-SOMO−1 → β-SUMO (98.37 %)
6	**1012.84 nm**	0.0097	α-SOMO →α-SUMO (81.837 %)
7	**956.95 nm**	0.0335	α-SOMO →α-SUMO+1 (87.643 %)
8	**827.20 nm**	0.0735	β-SOMO−5 →β-SUMO (77.695 %)
9	**754.18 nm**	0.0009	β-SOMO−6 →β-SUMO (89.755 %)
10	**718.86 nm**	0.0003	β-SOMO−9 →β-SUMO (85.643 %)
12	**618.26 nm**	0.0588	α-SOMO →α-SUMO+2 (81.837 %)
15	**547.81 nm**	0.0748	β-SOMO−11 →β-SUMO (68.022 %)

Table S4 List of the molecular orbitals for **[HTA]••**

Energy level	**[HTA]••**	**Energy level**	**[HTA]••**
***α*-SOMO** (-4.938 eV)	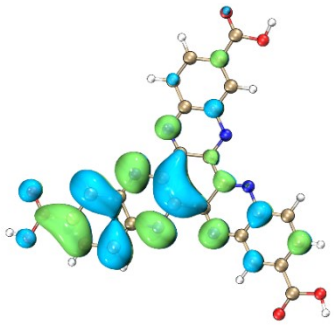	***β*-SOMO−11** (-8.459 eV)	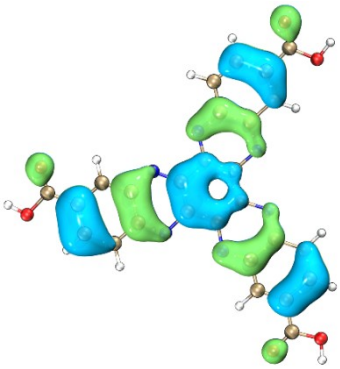
***α*-SUMO** (-3.076 eV)	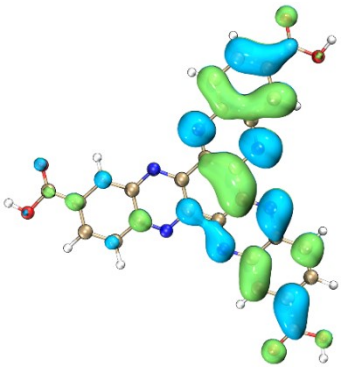	***β*-SOMO−9** (-8.209 eV)	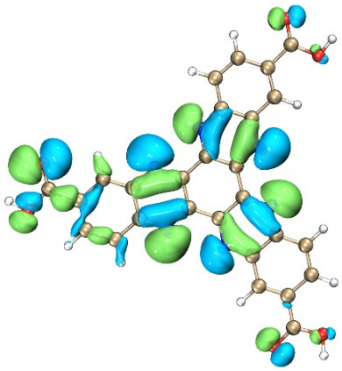
***α*-SUMO+1** (-3.005 eV)	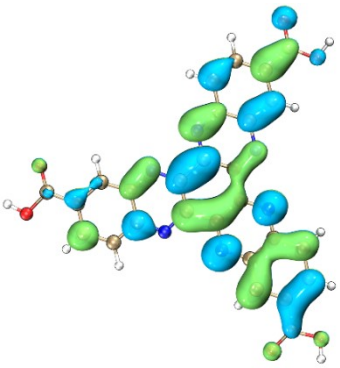	***β*-SOMO−6** (-7.758 eV)	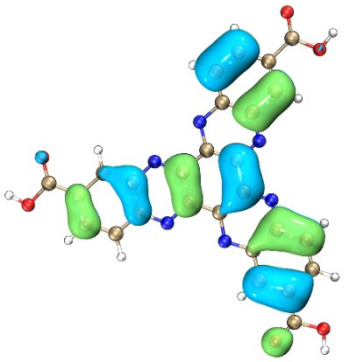
***α*-SUMO+2** (-1.945 eV)	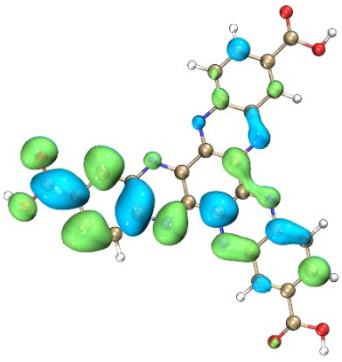	***β*-SOMO−5** (-7.503 eV)	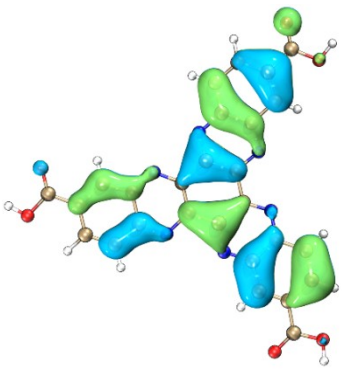

		β-SOMO−1 (-6.999 eV)	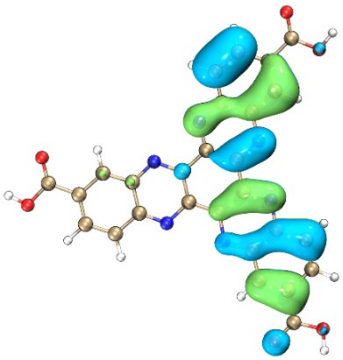
		β-SUMO (-5.506 eV)	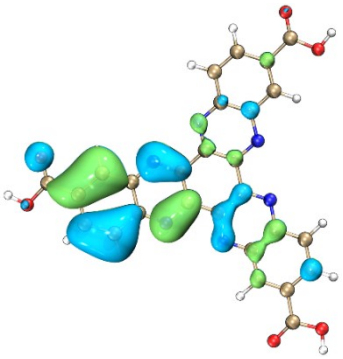

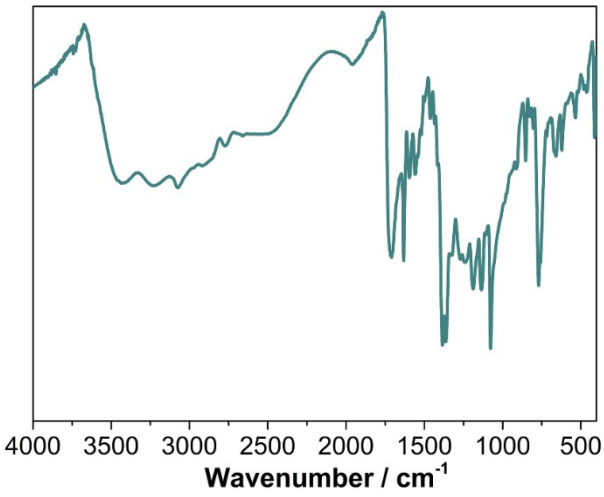

Fig. S1 IR spectrum of **HTA**.

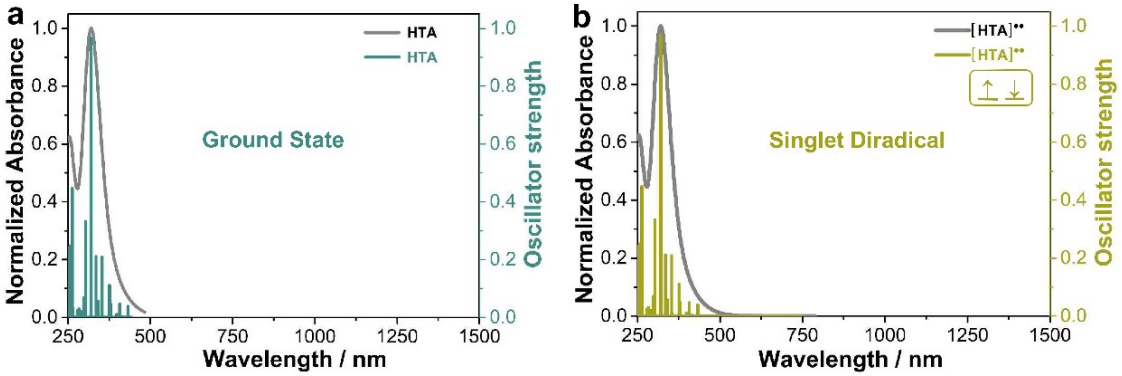

Fig. S2 Calculated optical absorption curves and lines of **HTA** based on ground state (a) and singlet diradical state (b).

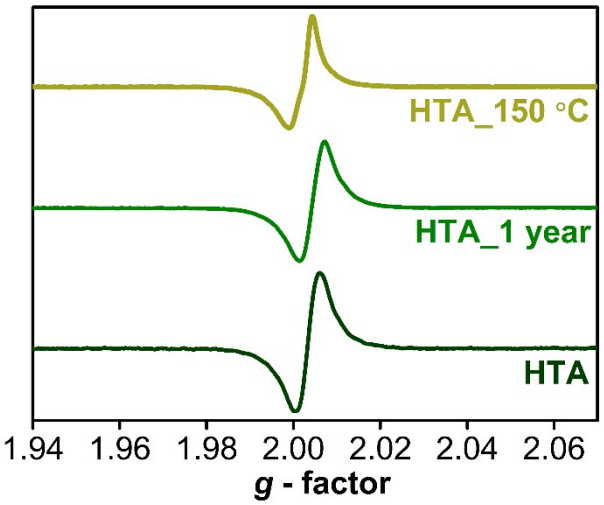

Fig. S3 Solid-state EPR spectra of **HTA** (dark green solid line), the sample **HTA** stored in air

for one year (green solid line) and the sample **HTA** after annealing at 150 °C for 12 hours (grass green solid line).

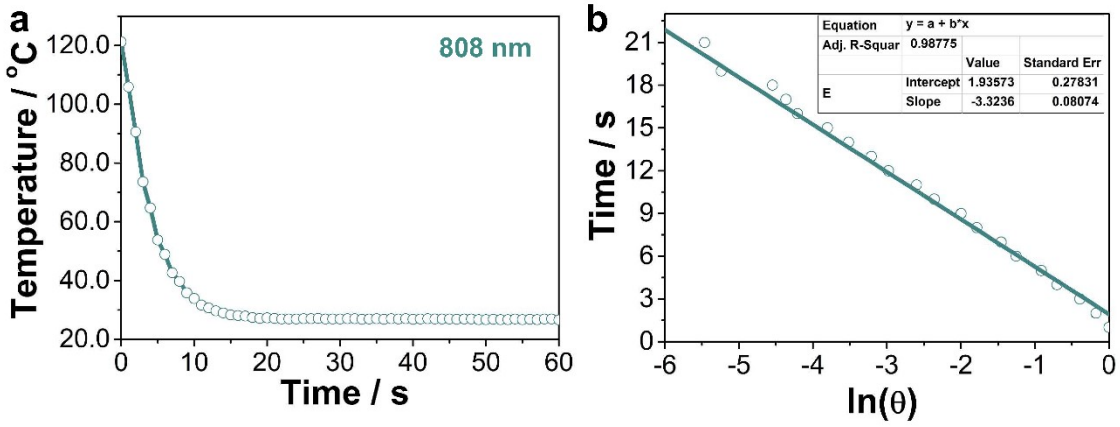

Fig. S4 Temperature decaying curve of compound **HTA** after removing the laser source of 808 nm (1.25 W/cm^2) (a) and the corresponding time-lnθ linear curve (b). The photothermal conversion efficiency (η_{808} = 71.09 %) was also calculated based on reported method[5]: $\eta_{808} = \frac{hS\Delta T_{max}}{I(1-10^{-A_{808}})}$, where the I is the laser power (1.25 W/cm^2), A_{808} is the absorbance of the samples at the wavelength of 808 nm (0.50, F(R)), and ΔT_{max} is the maximum temperature change (94.6 K). hs can be calculated based on the formula of $\tau_s = \frac{\sum_i m_i C_{p,i}}{hs}$, where τ_s is the sample system time constant, m_i (0.0159 g) and $C_{p,i}$ (1.33 J·(g·°C)$^{-1}$) are the mass and heat capacity of system components. When the laser turns off, τ_s can be estimated according to the formula: $t = -\tau_s ln\theta$. The θ can be obtained according to the formula: $\theta = \frac{T - T_{surr}}{T_{max} - T_{surr}}$, where T is the temperature of sample, T_{max} is the maximum system temperature, and T_{surr} is the environment temperature.

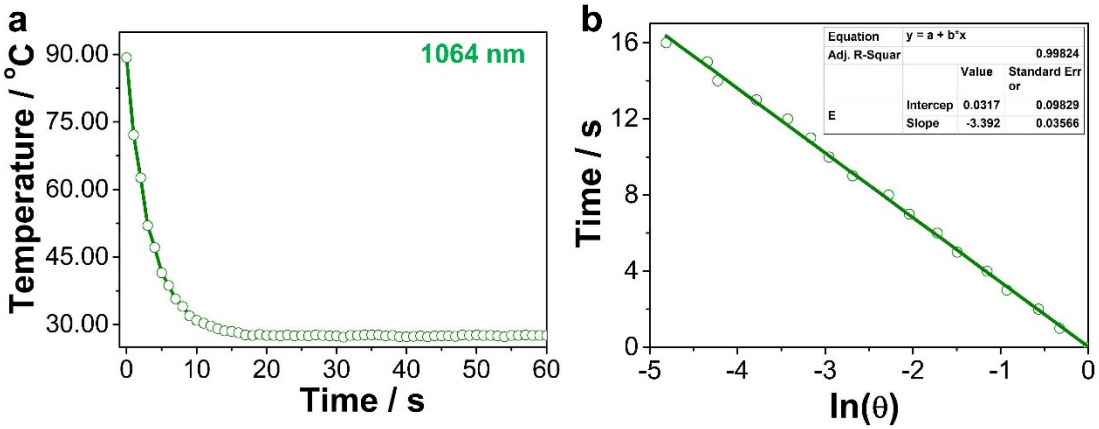

Fig. S5 Temperature decaying curve of compound **HTA** after removing the laser source of 1064 nm (1.25 W/cm^2) (a) and the corresponding time-lnθ linear curve (b). The photothermal conversion efficiency (η_{1064} = 61.68 %) was also calculated based on reported method[1]: $\eta_{1064} = \frac{hS\Delta T_{max}}{I(1-10^{-A_{1064}})}$, where the I is the laser power (1.25 W/cm^2), A_{1064} is the absorbance of the samples at the wavelength of 1064 nm (0.31, F(R)), and ΔT_{max} is the maximum temperature change (63.7 K). hs can be calculated based on the formula of $\tau_s = \frac{\sum_i m_i C_{p,i}}{hs}$, where τ_s is the sample system time constant, m_i (0.0159 g) and $C_{p,i}$ (1.33 J·(g·°C)$^{-1}$) are the mass and heat capacity of system components. When the laser turns off, τ_s can be estimated according to the formula: $t = -\tau_s ln\theta$. The θ can be obtained according to the formula: $\theta = \frac{T - T_{surr}}{T_{max} - T_{surr}}$, where T is the temperature of sample, T_{max} is the maximum system temperature, and T_{surr} is the environment temperature.

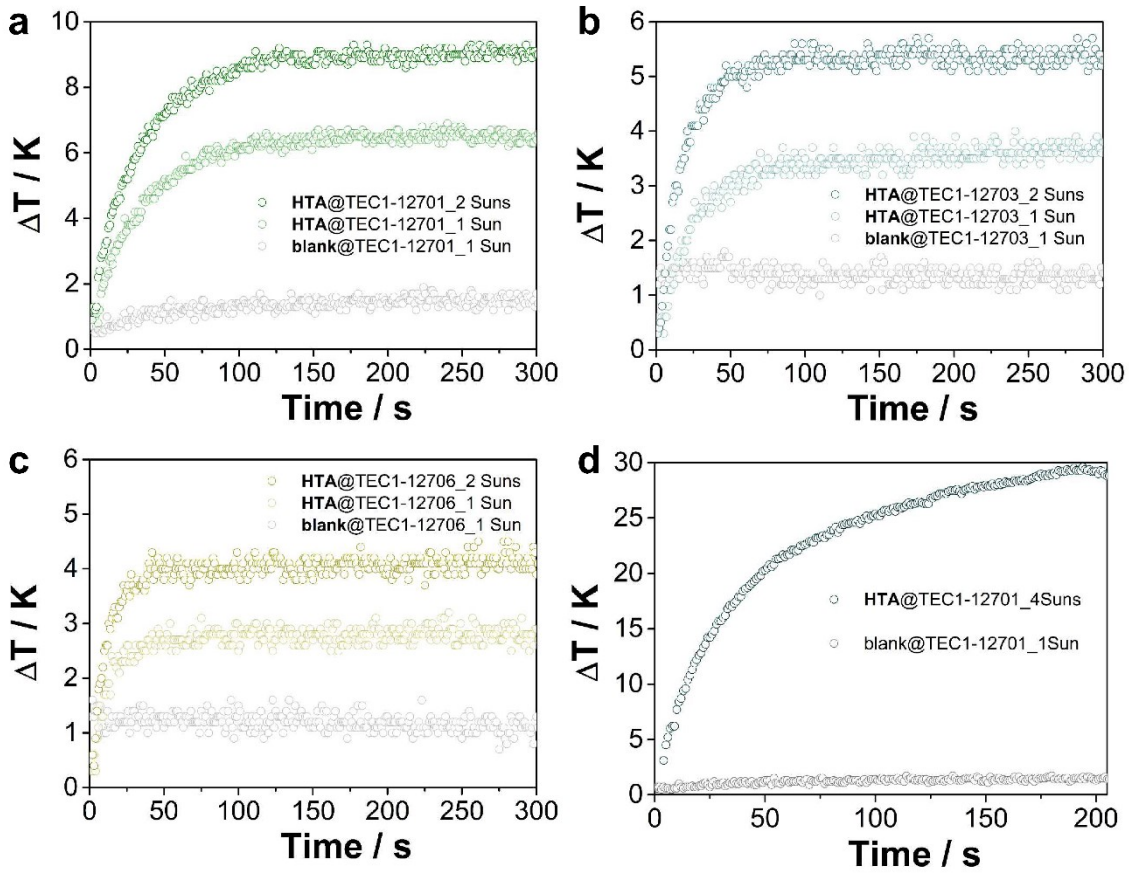

Fig. S6 (a-c) The temperature difference (ΔT) of different photo-thermo-electric conversion devices under the irradiation of 1 Sun and 2 Suns. (d) The temperature difference (ΔT) of **HTA**@TEC1-12701 under the irradiation of 4 Suns.

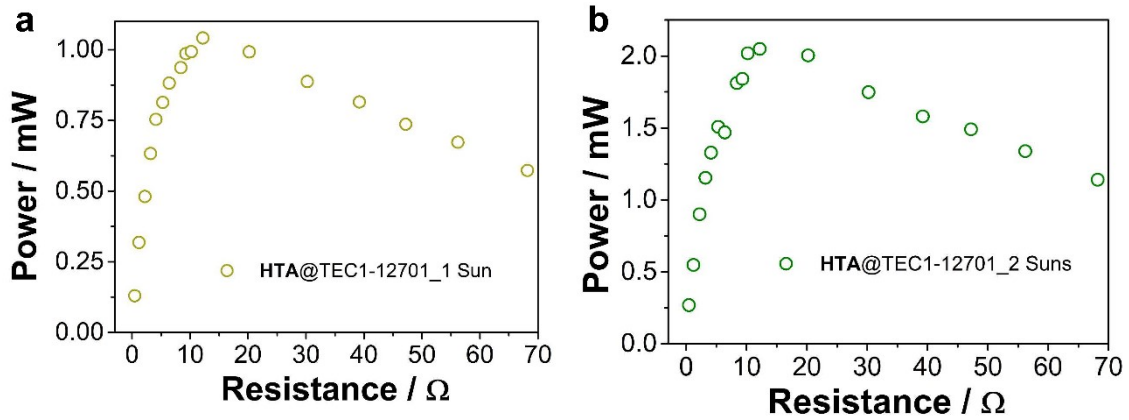

Fig. S7 Output power of **HTA**@TEC1-12701 under irradiation of 1 Sun (a) and 2 Suns (b) when loading different external resistances, respectively.

Movie S1.

A device **HTA**@TEC1-12701 drives a small fan under 4 Suns.

3. Reference

1. J. Wang, K. Tee, Y. Lee, S. N. Riduan and Y. Zhang, Hexaazatriphenylene derivatives/GO composites as organic cathodes for lithium ion batteries. *J. Mater. Chem. A* 2018, **6**, 2752–2757.

2. L. A. Curtiss, P. C. Redfern, K. Raghavachari, J. A. Pople, Gaussian-3X (G3X) theory: Use of improved geometries, zero-point energies, and Hartree–Fock basis sets. *J. Chem. Phys.* 2001, **114**, 108–117.

3. M. J. Frisch, G. W. Trucks, H. B. Schlegel, G. E. Scuseria, M. A. Robb, J. R. Cheeseman, G. Scalmani, V. Barone, G. A. Petersson, H. Nakatsuji, X. Li, M. Caricato, A. V. Marenich, J. Bloino, B. G. Janesko, R. Gomperts, B. Mennucci, H. P. Hratchian, J. V. Ortiz, A. F. Izmaylov, J. L. Sonnenberg, D. Williams-Young, F. Ding, F. Lipparini, F. Egidi, J. Goings, B. Peng, A. Petrone, T. Henderson, D. Ranasinghe, V. G. Zakrzewski, J. Gao, N. Rega, G. Zheng, W. Liang, M. Hada, M. Ehara, K. Toyota, R. Fukuda, J. Hasegawa, M. Ishida, T. Nakajima, Y. Honda, O. Kitao, H. Nakai, T. Vreven, K. Throssell, J. A. Montgomery Jr., J. E. Peralta, F. Ogliaro, M. J. Bearpark, J. J. Heyd, E. N. Brothers, K. N. Kudin, V. N. Staroverov, T. A. Keith, R. Kobayashi, J. Normand, K. Raghavachari, A. P. Rendell, J. C. Burant, S. S. Iyengar, J. Tomasi, M. Cossi, J. Millam, M. Klene, C. Adamo, R. Cammi, J. W. Ochterski, R. L. Martin, K. Morokuma, O. Farkas, J. B. Foresman and D. J. Fox, *Gaussian 16, Rev. C.01*, Gaussian, Inc., Wallingford CT, 2016.

4. T. Lu, F. W. Chen, Multiwfn: A multifunctional wavefunction analyzer. *J. Comput. Chem.* 2012, **33**, 580–592.

5. S. Wang, S. Li, J. Xiong, Z. Lin, W. Wei, Y. Xu, Near-infrared photothermal conversion of stable radicals photoinduced from a viologen-based coordination polymer. *Chem. Commun.* 2020, **56**, 7399–7402.